Nonlinear Phenomena in Complex Systems, vol. **28**, no. 2 (2025), pp. 155 - 166

Quarks, Gluons and Ghosts at Finite Temperatures within a Bethe–Salpeter–Dyson–Schwinger Approach

L. P. Kaptari*
Bogoliubov Laboratory of Theoretical Physics,
Joint Institute for Nuclear Research, Dubna, Moscow Region, 141980, RUSSIA

O. P. Solovtsova†
Gomel State Technical University, Gomel, 246746, BELARUS,
Bogoliubov Laboratory of Theoretical Physics,
Joint Institute for Nuclear Research, Dubna, Moscow Region, 141980 RUSSIA
(Received 2 April, 2025)

A framework based on the rainbow approximation to the Dyson–Schwinger and Bethe–Salpeter equations with effective parameters adjusted to lattice data is suggested to calculate the masses of the ground and excited states of mesons and pseudo-scalar glueballs as QCD bound states of quarks and gluons. The structure of the truncated Bethe–Salpeter equation with the gluon and ghost propagators as solutions of the truncated Dyson–Schwinger equations is analysed in the Landau gauge. Both the Bete–Salpeter and Dyson–Schwinger equations are solved numerically within the same rainbow-ladder truncation with the same effective parameters which ensure consistency of the approach. We found that with a set of parameters, which provides a good description of the lattice data within the Dyson–Schwinger approach, the solutions of the Bethe–Salpeter equation for mesons and pseudo-scalar glueballs exhibit a rich mass spectrum that also includes the ground and excited states predicted by the lattice calculations. The obtained mass spectrum contains also several intermediate excitations unexpected within the lattice approaches.

PACS numbers: 11.10.St, 14.70.Dj, 12.38.Lg, 12.39.Mk
Keywords: bound and unstable states, Bethe–Salpeter equations, rainbow approximation, gluons, glueball, rainbow-ladder truncation, nonstandard multi-quark/gluon states contributions
DOI: https://doi.org/10.5281/zenodo.15745818

1. Introduction

Quantum Chromodynamics (QCD) as the fundamental theory of strong interaction is aimed to describe the quark-gluon structure of the nuclear matter from the most general first principles. Due to the asymptotic freedom of QCD, quarks and gluons essentially become free in hot nuclear matter. The current understanding of QCD suggests that at large values of the density ρ or/and of the chemical potential μ one expects a true phase transition from a confined (hadronic) to a deconfined (plasma) phase, usually referred to as the quark-gluon plasma (QGP). In such phases confinement is absent and the characteristics of systems with strong interacting particles are qualitatively different in comparison to their vacuum properties. The study of the behaviour of hadrons in hot and dense nuclear matter is among the most interesting and challenging problems intensively investigated by theorists and experimentalists. It is commonly adopted that QGP existed in the early universe and can also be briefly produced in the laboratory by heavy-ion collisions.

In this paper we present our recent results on QCD bound states, mesons, and glueballs, within an approach based on Dyson–Schwinger

*E-mail: `kaptari@theor.jinr.ru`
†E-mail: `solovtsova@gstu.gomel.by;olsol@theor.jinr.ru`

and Bethe–Salpeter equations at zero and finite temperatures. Among other approaches related to the study of QGP one can mention lattice QCD simulations [1–9] complemented by functional renormalization group (FRG) methods (see, e.g., Refs. [10, 11]), approaches based on QCD Sum Rules [12, 13], and functional approaches via the Dyson–Schwinger equations [14] (for a review of different methods in studying gauge bosons at zero and finite temperatures, see Refs. [15, 16]). Despite a fairly rigorous theoretical foundation, these approaches are rather complex and cumbersome in further applications in describing the temperature dependence of physical bound states, such as mesons and glueballs, for example. It is tempting therefore to elaborate transparent models which, on the one hand, are simple and physically understandable and, on the other hand, cover the main characteristics of the phenomena studied. Hereinbelow we employ a generalization of the well-known rainbow approximation to the truncated Dyson–Schwinger equations (tDSE) [17–20] to finite temperatures in Euclidean space within the imaginary-time formalism [20–24] and employ the corresponding solution to tDSE in the Bethe–Salpeter equations for mesons and glueballs.

2. Basic Formulae

2.1. Truncated Dyson–Schwinger and Bethe–Salpeter equations in vacuum

The Bethe–Salpeter equations (in the ladder approximation) for glueballs, ghosts and mesons are presented bellow in Fig. 1 as three Feynman diagrams. Wiggly, dotted and solid lines stand for gluon, ghost, and quark propagators, respectively. The irreducible one-particle vertices and the full propagators are represented and marked by filled blobs.

To solve this system numerically, we need information on the nonperturbative propagators of quarks, gluons, and ghosts and their properties in complex Euclidean momentum space. This

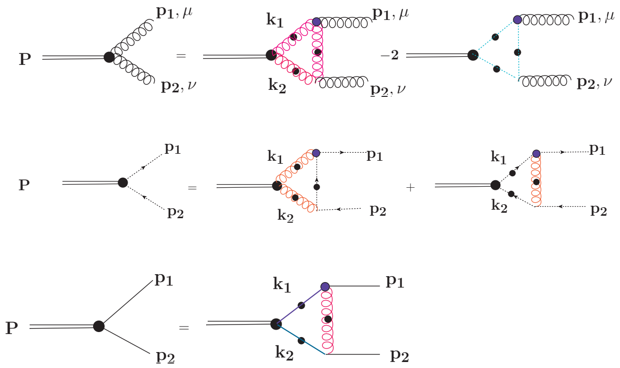

FIG. 1. (color online) Diagrammatic representation of the Bethe–Salpeter equation for glueball (upper panel), ghost (middle panel), and meson (lower panel) bound states. The irreducible one-particle vertices and the full propagators are represented and marked by filled blobs. Wiggly, dotted and solid lines stand for gluons, ghosts and quarks, respectively. The irreducible one-particle vertices and the full propagators are represented and marked by filled blobs.

can be achieved, e.g., by solving the coupled truncated Dyson–Schwinger equations for the corresponding propagators along the real axis of the momentum and then using the tDSE equations at complex external momenta corresponding to the propagators entering into the BS equations. Schematically, the system of Dyson–Schwiner equations is depicted in Fig. 2.

Direct calculations of the amplitudes of the homogeneous Bethe–Salpeter equations for mesons and glueballs, shown in Fig. 1, lead to

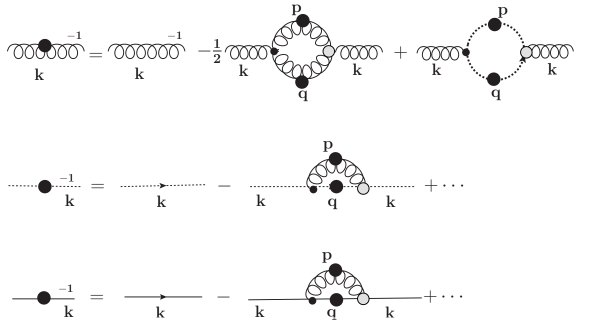

FIG. 2. The system of Dyson–Schwinger equations for gluon (upper panel), ghost (middle panel) and quark (lower panel) propagators. Wiggly, dotted and solid lines stand for gluons, ghosts and quarks, respectively. The irreducible one-particle vertices and the full propagators are represented and marked by filled blobs.

$$\Gamma(P,p) = -\frac{4}{3}\int \frac{d^4k}{(2\pi)^4}\gamma_\mu S(\eta_1 P + k)\Gamma(P,k)S(-\eta_2 P + k))\gamma_\nu \left[g^2 D_{\mu\nu}(p-k)\right], \tag{1}$$

$$A_{\mu\nu}(p_1,p_2) = \quad D_{\mu\mu_1}(p_1)\left(-N_c\int \frac{d^4k}{(2\pi)^4}\Gamma_1^{\mu_1\alpha\lambda}(p_1,k_1,\kappa)A_{\alpha\beta}(k_1,k_2)\Gamma_2^{\nu_1\beta\lambda_1}(p_2,k_2,\kappa)D_{\lambda\lambda_1}(\kappa)\right)D_{\nu\nu_1}(p_2), \tag{2}$$

where Eq. (1) refers to meson while Eq. (2) to glueball bound states. The quark and antiquark propagators are denoted as $S(\eta_1 P + k)$ and $S(-\eta_2 P + k))$, respectively, with $\eta_1 + \eta_2 = 1$; $\Gamma_1^{\mu_1\alpha\lambda}(,k,\kappa)$ is the three-gluon vertex. Eventually, the gluon propagators are denoted as $D_{\mu\nu}(p)$. It should be noted that for pseudoscalar glueballs only the first diagram in Fig. 1 contributes to the gg-bound state.

The required gluon and ghost propagators are obtained by direct calculation of the corresponding one-loop Feynman diagrams for the tDSE, cf. Fig. 2. In the Landau gauge, the resulting system can be written as

$$D^{-1}_{\mu\nu}(k_4^2,\mathbf{k}^2) = Z_3 D^{-1}_{0\,\mu\nu}(k^2) + \Sigma^{gluon}_{\mu\nu}(k_4^2,\mathbf{k}^2) + \Sigma^{ghost}_{\mu\nu}(k_4^2,\mathbf{k}^2) \tag{3}$$

$$D^{-1}_{G}(k_4^2,\mathbf{k}^2) = \tilde{Z}_3 D^{-1}_{0G}(k^2) + S^{ghost}(k_4^2,\mathbf{k}^2) \tag{4}$$

$$S^{-1}(k) = S_0^{-1}(k) + \frac{4}{3}\int \frac{d^4q}{(2\pi)^4}\gamma_\mu S(q)\gamma_\nu \times\left[g^2 D^{\mu\nu}(k-q)\right] + \cdots, \tag{5}$$

where Z_3 and $\tilde{Z}_3$ are the gluon and ghost renormalization constants, respectively, $S_0(k^2)$, $D_{0\,\mu\nu}(k^2)$, and $D_{0G}(k^2)$ are the quark, gluo, and ghost free propagators, $k^2 = k_4^2 + \mathbf{k}^2$ and $\Sigma^{gluon}_{\mu\nu}(k_4,\mathbf{k})$, $\Sigma^{ghost}_{\mu\nu}(k_4,\mathbf{k})$ and $S^{ghost}(k_4,\mathbf{k})$ correspond to the self-energy terms of the first two tDSE depicted in Fig. 2.

3. Rainbow approximation

Attempts to solve the system of coupled equations by employing directly the QCD Feynman rules encounter difficulties related to regularizations of divergent loop integrals and to symmetry constraints on gluon-ghost and three-gluon vertices, such as Slavnov–Taylor identities. Clearly, further approximations are required. A rigorous analysis of the tDSE has been presented in a series of publications in Refs. [25, 26] (see also the review Ref. [27] and references therein quoted). All the mentioned approaches result in rather cumbersome expressions for the system of tDSE's which, consequently, cause difficulties in finding numerical solutions. Moreover, these circumstances are more significant in attempts to solve the tDSE at finite temperatures. In order to avoid the mentioned difficulties and simplify the angular integrations, in the present paper we employ a rainbow-like approximation similar to the rainbow model [17, 18, 21–23] for the interaction kernels. This approximation consists in replacing the dressed vertices together with the dressed exchanging propagators by their bare quantities augmented by some effective form factors.

Following examples in the literature [19], the interaction kernel for the quark tDSE in the rainbow approximation in the Landau gauge is chosen as

$$g^2(k^2)\mathcal{D}_{\mu\nu}(k^2) = \frac{4\pi^2 D k^2}{\omega^6} e^{-k^2/\omega^2}\left(\delta_{\mu\nu} - \frac{k_\mu k_\nu}{k^2}\right) \tag{6}$$

with $D = 16$ GeV^2 and $\omega = 0.5$ GeV.

For the gluon and ghost tDSE one has

$$\frac{g^2}{4\pi}\Gamma^{(0)}_{\mu_1\alpha\lambda}(p_1,k_1,\kappa)D^{\lambda\lambda_1}(\kappa^2)\Gamma_{\nu_1\beta\lambda_1}(p_2,k_2,\kappa) = \Gamma^{(0)}_{\mu_1\alpha\lambda}(p_1,k_1,\kappa)t^{\lambda\lambda_1}(\kappa)\Gamma^{(0)}_{\nu_1\beta\lambda_1}(p_2,k_2,\kappa)F_1^{eff}(p^2), \tag{7}$$

$$\frac{g^2}{4\pi}D_G(p^2)\Gamma_\nu(p) = \Gamma^{(0)}_\nu(p)F_2^{eff}(p^2), \tag{8}$$

$$\frac{g^2}{4\pi}\Gamma^{(0)}_\mu(q)D^{\mu\nu}(p^2)\Gamma_\nu(k,q,p) = \Gamma^{(0)}_\mu(q)t^{\mu\nu}(p)\Gamma^{(0)}_\nu(k)F_3^{eff}(p^2), \tag{9}$$

where the above three terms correspond to the three loop diagrams in Fig. 2. Since we are interested in bound states, i.e. mostly in the range of internal momenta corresponding to the infra-red region, in the present paper we use for $F^{eff}(p^2)$ the Gaussian form with two terms for $F^{eff}_{1,3}(p^2)$ as in [28]. This is quite sufficient to obtain a reliable solution to the system of tDS equations. Such a Gaussian representation of the interaction kernels has been widely employed previously for quarkonia and is known as the AWW kernel [17].

Explicitly, in Euclidean space the effective form factors are chosen as

$$F_1(p^2) = D_{11}\frac{p^2}{\omega_{11}^6}e^{-p^2/\omega_{11}^2} + D_{12}\frac{p^2}{\omega_{12}^6}e^{-p^2/\omega_{12}^2}, \tag{10}$$

$$F_2(p^2) = \frac{D_{21}}{\omega_{21}^4}e^{-p^2/\omega_{21}^2} + \frac{D_{22}}{\omega_{22}^4}e^{-p^2/\omega_{22}^2}, \tag{11}$$

$$F_3(p^2) = D_{31}\frac{p^2}{\omega_{31}^6}e^{-p^2/\omega_{31}^2} + D_{32}\frac{p^2}{\omega_{32}^6}e^{-p^2/\omega_{32}^2}. \tag{12}$$

The solution to this system is found numerically by utilization of an iteration procedure. To this end, the integral equation is replaced by the Gaussian quadrature formula resulting in a system of algebraic equations with respect to the corresponding Gaussian nodes. The effective parameters are those as reported in Ref. [28]: $D_{11} = 0.462$ GeV^2, $D_{12} = 0.116$ GeV^2,

$\omega_{11} = 1.095$ GeV, $\omega_{12} = 2.15$ GeV for the 3-gluon loop, $D_{21} = 7.7$ GeV^2, $D_{22} = 0.25$ GeV^2, $\omega_{21} = 0.58$ GeV, $\omega_{22} = 4.5$ GeV, for the ghost loop and $\omega_{31} = 0.73$ GeV, $\omega_{32} = 2.16$ GeV, $D_{31} = 0.39\pi$ GeV^2, $D_{32} = 0.1\pi$ GeV^2 for the ghost-gluon loop (cf. the three loops in Fig. 2).

Then, with these parameters we have solved the tDSE in the complex plane corresponding to the domain of definition of the propagators entering into the BS equations. The latter was also solved numerically for mesons and glueballs. Each solution defines the ground or exited state of the mesons or glueballs. The results of calculations of the quarkonia (meson) and glueball mass spectrum are presented in Fig. 3 where the bars indicate the calculated bound state masses. It is seen that with the chosen effective parameters the calculated mass spectrum describes rather well the available experimental data.

4. Finite temperatures

At finite temperatures, within the imaginary time formalism, all the relevant four-momenta in Euclidean space possess discrete spectra of their fourth components, $k_4 = \Omega_n$ ($n \subset \mathbb{Z}$), where $\Omega_n = 2\pi nT$ for bosons (gluons) and $\Omega_n = \pi(2n+1)T$ for fermions (quarks). As for the Fadeev–Popov ghosts, in spite of the Grassmann nature of their fields needed in the gauge fixing procedure, ghosts are formally related to (nonexisting) spin-zero particles and to scalar propagators. Consequently, ghost fields satisfy periodic conditions like any bosonic field, cf. Refs. [16, 29–31], so that the Matzubara frequencies for ghosts are even[a]

$$\int\limits_{-\infty}^{\infty} \frac{dq_4}{2\pi} \int \frac{d^3q}{(2\pi)^3} f(q_4, \mathbf{q})$$
$$\to T \sum_{n=-\infty}^{\infty} \int \frac{d^3q}{(2\pi)^3} f(\Omega_n, \mathbf{q}). \qquad (13)$$

[a] There was some confusion in the literature about the ghost Matsubara frequency, see Ref. [32].

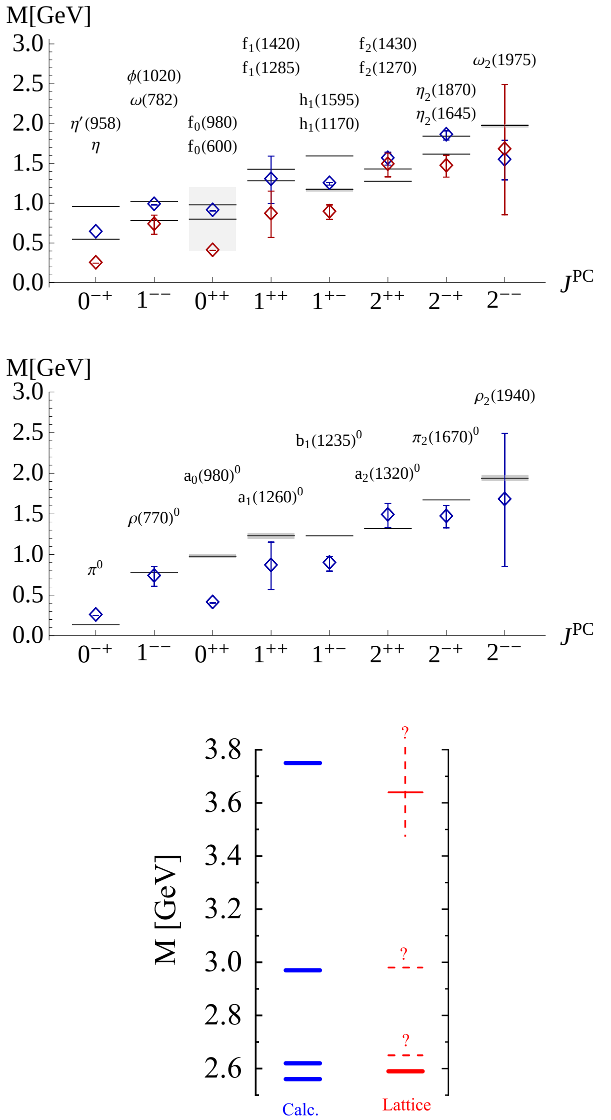

FIG. 3. (color online) Mass spectrum of the low-lying isoscalar (upper panel) and isovector (middle panel) mesons, respectively, vs. the available experimental data. Lower panel: our predictions for the ground and exited states of pseudo-scalar glueballs (solid lines, labeled as "Calc.") vs. the lattice QCD calculations, solid lines ("Lattice") for the firmly confirmed results, and the lines ("Lattice") for preliminary, unconfirmed results.

In the Landau gauge, the Euclidean quark $S(k^2)$ propagators are expressed via the mass parameter $B(p_4, \mathbf{p})$ and field renormalization functions $A(p_4,\mathbf{p})$ and $C(p_4,\mathbf{p})$

$$S^{-1}(p_4,\mathbf{p}^2)=\left[i\gamma\cdot\mathbf{p}A(p_4,\mathbf{p}^2)+i\gamma_4p_4C(p_4,\mathbf{p}^2)+B(p_4,\mathbf{p}^2)\right]^{-1}. \quad (14)$$

The gluon propagator $\mathcal{D}^{ab}_{\mu\nu}(k_4,\mathbf{k})$ and ghost propagator $\mathcal{D}^{ab}_{G}(k_4,\mathbf{k})$ are also defined by the renormalization (dressing) functions $Z(k_4,\mathbf{k})$ and $G(k_4,\mathbf{k})$ as

$$\mathcal{D}^{ab}_{\mu\nu}(k)=\delta^{ab}D_{\mu\nu}(k_4,\mathbf{k})=\delta^{ab}\left\{\frac{Z_T(k_4,\mathbf{k})}{k^2}\mathcal{P}^T_{\mu\nu}(\mathbf{k})+\frac{Z_L(k_4,\mathbf{k})}{k^2}\mathcal{P}^L_{\mu\nu}(k_4,\mathbf{k})\right\}, \quad (15)$$

$$\mathcal{D}^{ab}_{G}(k_4,\mathbf{k})=-\delta^{ab}D_G(k_4,\mathbf{k})=-\delta^{ab}\frac{G(k_4,\mathbf{k})}{k^2}, \quad (16)$$

where $\mathcal{P}^L_{\mu\nu}(k_4,\mathbf{k})$, and $\mathcal{P}^T_{\mu\nu}(\mathbf{k})$ denote the longitudinal and transversal, in 3D space, projectors

$$\mathcal{P}^T_{\mu\nu}(\mathbf{k})=\begin{cases}0, & \mu \text{ and/or } \nu=4,\\ \delta_{\alpha\beta}-\dfrac{k_\alpha k_\beta}{\mathbf{k}^2}; & \mu,\nu=\alpha,\beta=1,2,3,\end{cases} \quad (17)$$

$$\mathcal{P}^L_{\mu\nu}(k)=\mathcal{P}_{\mu\nu}(k)-\mathcal{P}^T_{\mu\nu}(\mathbf{k}), \quad (18)$$

where $\mathcal{P}_{\mu\nu}(k)=\delta_{\mu\nu}-\dfrac{k_\mu k_\nu}{k^2}$.

Then Eq. (15) reads as

$$\frac{k^2}{Z_T(k_4,\mathbf{k})}\mathcal{P}^T_{\mu\nu}(\mathbf{k})+\frac{k^2}{Z_L(k_4,\mathbf{k})}\mathcal{P}^L_{\mu\nu}(k_4,\mathbf{k})= Z_3k^2\mathcal{P}_{\mu\nu}(k)+\Sigma^{gluon}_{\mu\nu}(k_4^2,\mathbf{k}^2)+\Sigma^{ghost}_{\mu\nu}(k_4^2,\mathbf{k}^2). \quad (19)$$

After contracting the color indices in the corresponding loops in Fig. 2, the self-energy parts acquire the explicit form as

$$\frac{k^2}{Z_T(k_4,\mathbf{k})}\mathcal{P}^T_{\mu\nu}(\mathbf{k})+\frac{k^2}{Z_L(k_4,\mathbf{k})}\mathcal{P}^L_{\mu\nu}(k_4,\mathbf{k})=Z_3k^2\mathcal{P}_{\mu\nu}(k)+\Sigma^{gluon}_{\mu\nu}(k_4^2,\mathbf{k}^2)+\Sigma^{ghost}_{\mu\nu}(k_4^2,\mathbf{k}^2), \quad (20)$$

$$\Sigma^{gluon}_{\mu\nu}(\Omega_n,\mathbf{k})=\frac{1}{2}\frac{3T}{2\pi^2}\sum_m\int d^3q\Gamma^{(0)}_{\mu\alpha\rho}(k,-q,p)\frac{Z_T(\Omega_m,\mathbf{q})\mathcal{P}^T_{\alpha\beta}(\mathbf{q})+Z_L(\Omega_m,\mathbf{q})\mathcal{P}^L_{\alpha\beta}}{q^2}\times\left[\frac{g^2}{4\pi}\Gamma_{\beta\nu\sigma}(q,-p,-k)\left(D_T(\Omega_{mn},\mathbf{p})\mathcal{P}^T_{\sigma\rho}(\mathbf{p})+D_L(\Omega_{mn},\mathbf{p})\mathcal{P}^L_{\sigma\rho}(p)\right)\right], \quad (21)$$

$$\Sigma^{ghost}_{\mu\nu}(\Omega_n,\mathbf{k})=-\frac{3T}{2\pi^2}\sum_m\int d^3q\frac{G(\Omega_m,\mathbf{q})}{q^2}\left[\Gamma^{(0)}_\mu(q)\frac{g^2}{4\pi}D_G(\Omega_{mn},\mathbf{p})\Gamma_\nu(p)\right], \quad (22)$$

$$S^{ghost}(\Omega_n,\mathbf{k})=\frac{3T}{2\pi^2}\sum_m\int d^3q\Big[\frac{g^2}{4\pi}\Gamma^{(0)}_\mu(q)D_{\mu\nu}(p^2)\Gamma_\nu(k,q,p)\Big]\frac{G(\Omega_m,\mathbf{q})}{q^2}, \quad (23)$$

where $p=q-k$, $p_4\equiv\Omega_{mn}=\Omega_m-\Omega_n$, $\mathbf{p}=\mathbf{q}-\mathbf{k}$ and the terms enclosed in the square brackets define the interaction kernel of the corresponding integral equation.

The tDSE for the scalar dressing functions $Z_{T,L}$ are obtained from the tDSE (3) by inserting Eqs. (21)-(22) into Eq. (3), multiplying the left and right hand sides consecutively by $\mathcal{P}^T(\Omega_n,\mathbf{k})$ and $\mathcal{P}^L(\Omega_n,\mathbf{k})$ and contracting all the Lorentz indices.

The gluon renormalization constants $Z_{3(T,L)}$ for the transverse and longitudinal propagators, in principle, can be different and must be determined separately. In the present paper, for the sake of simplicity, we adopt the renormalization constant Z_3 to be the same for both transverse and longitudinal parts. Moreover, the concrete numerical values for Z_3 and $\tilde{Z}_3$ are taken from the previous fit [28] of the tDSE solution in vacuum to the lattice QCD data, viz. $Z_3 = \tilde{Z}_3 \approx 1.065$.

The effective parameters in (10)-(12) can generally be different for the transversal (T) and longitudinal (L) parts. In addition, all parameters, including the renormalization constants, $\tilde{Z}_3$ and Z_3, may depend on the temperature T and Matsubara frequency Ω_n, see Ref. [33]. However, as observed in Refs. [24, 34, 35], at low temperatures the interaction kernel is insensitive to the temperature impact and, as a first approximation, the interaction kernels can be chosen the same as at $T = 0$ with $D^T = D^L$ and $\omega_i^T = \omega_i^L$. For larger temperatures such a choice of transversal and longitudinal effective parameters is less justified.

We have solved the mentioned system of equations for the quantities $A(p_4, \mathbf{p})$, $C(p_4, \mathbf{p})$ and $B(p_4, \mathbf{p})$ for the quark propagators Eq. (14) and for the dressing functions $Z_T(p_4, \mathbf{p})$, $Z_L(p_4, \mathbf{p})$ and $G(p_4, \mathbf{p})$, Eqs. (20)-(23), numerically by an iteration procedure. The number of Matsubara frequencies has been fixed in the interval $(-30 \leq n \leq 30)$, and the Gaussian mesh for the spatial integration on $|\mathbf{k}|^2$ consisted of 72 nodes with the upper limit of integration $|\mathbf{k}|^2 \sim 220$ GeV^2/c^2. To obtain more dense Gaussian nodes at low $|\mathbf{k}|^2$, an appropriate mapping has been employed. The current quark mass in tDSE is taken $m_0 = 5$ MeV for the u and d-quarks. In the chiral limit $m_0 = 0$ MeV, the exact zeros of the dynamical quark mass $M(T_c) = B(T_c)/A(T_c) = 0$ and/or quark condensate $\langle q\bar{q}\rangle = 0$ determine the true phase transition with chiral symmetry restoration. In our case $T_c \sim 110$ MeV.

4.1. Meson dissociation at $T > T_c$

The solution to the quark propagator was included into the BS equation to solve it for pseudoscalar mesons at finite temperature.

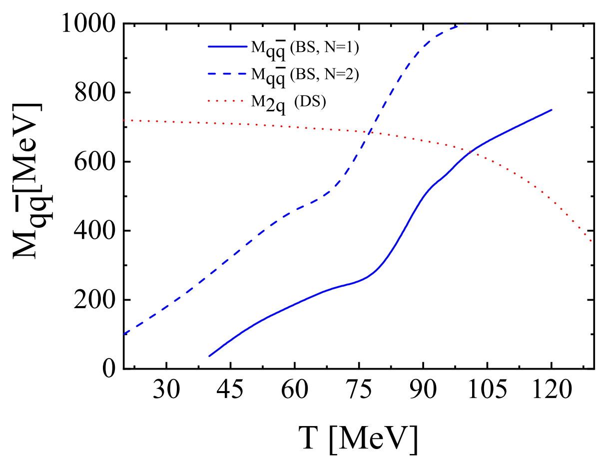

FIG. 4. (color online) The mass of the pseudoscalar meson as a function of the temperature T. Solid and dashed curves correspond to the lowest values of the Matsubara frequencies, N=1 and N=2, respectively. Dotted curve is the mass of two quarks as the solution of the temperature dependent Dyson–Schwinger equation. Below this curve, two quarks are in an bound states $M_{q\bar{q}} < m_q + m_{\bar{q}}$, above it indicates that the mesons are in the excited state with a positive binding energy $M_{q\bar{q}} > m_q + m_{\bar{q}}$, i.e. the meson dissociates into two quasi-free quarks.

The results of calculations of the meson mass for two lowest values of the Matsubara are presented in Fig. 4. The dotted line represents the dependence of the mass of two free quarks on temperature. The dashed and solid lines are the two-quark (quarkonia) bound states in dependence on the temperature T at two lowest Matsubara frequencies. From the figure one infers that below the dotted line the mass of quarkonia is less than the mass of two free constituents, i.e. the quarkonia appear to be a rather stable bound state. At a temperature of $T \gtrsim 110$ MeV, the bound state dissociates into a hot quark-gluon like phase.

4.2. Solution to the ghost dressing function $G(k_4, \mathbf{k}^2)$

The results of calculations are presented in Fig. 5 where we exhibit the temperature dependence of the ghost dressing function $G(k_4, \mathbf{k}^2)$. The left panel illustrates the dressing function at the zero Matsubara frequency, $n = 0$, as a function of the three-momentum $\mathbf{k}^2$ at two values of the temperature, $T = 10$ MeV and $T = 150$ MeV. As expected, the temperature dependence is rather weak for all values of $\mathbf{k}^2$, except for the vicinity of very low momenta $\mathbf{k}^2 \sim 0$ and is quite similar to the behaviour of $G(k^2)$ at $T = 0$, cf. Ref [28].

In the right panel, we present the temperature dependence of the dressing function $G(k_4, \mathbf{k}^2)$ at $\mathbf{k}^2 = 0$ and two values of the Matsubara frequencies, $n = 0$ and $n = 1$. Since the fourth component of the ghost momentum strongly depends on the Matsubara frequency, $k_4^2 = [2n\pi T]^2$, the dressing function $G(k_4, 0)$ is also quite sensitive to T and n. This qualitatively agrees with the lattice QCD calculations reported in Ref. [3, 34, 35] where it was found that at low enough three-momenta $|\mathbf{k}|$ and $T/T_c < 1.4$ the ghost dressing function $G(k_4, \mathbf{k})$ changes rather weakly with the temperature at $k_4 = 0$ and decreases as k_4 increases. As seen from Fig. 5, the dressing function is basically temperature independent, i.e. $\frac{d}{dT}G(0,0) \sim 0$, up to $T = T_0 \simeq 150$ MeV. At $T > T_0$ the function changes its concavity (the second derivative w.r.t. temperature changes the sign) and sharply increases. In some sense, T_0 can be considered as a critical point for the temperature dependence of the ghost dressing $G(0,0)$. The ghost dressing for the non-zero Matsubara modes smoothly decreases with T and does not exhibit any irregularities.

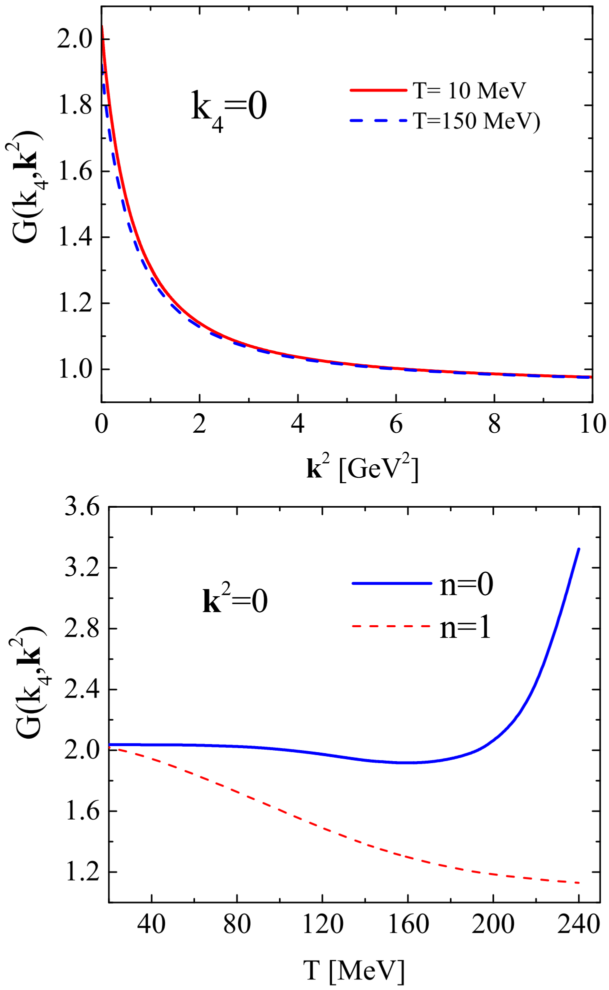

FIG. 5. (color online) The solution of the Dyson–Schwinger equation for the ghost dressing function $G(k_4, \mathbf{k}^2)$. Left panel: dependence on the three-momentum squared $\mathbf{k}^2$ at the zero Matsubara frequency, $n = 0$, for two values of the temperature $T = 10$ MeV (solid curve) and $T = 150$ Mev (dashed curve). Right panel: temperature dependence of the dressing function at the zero three-momentum $\mathbf{k}^2 = 0$ and two values of the Mastubara frequency, $n = 0$ (solid curve) and $n = 1$ (dashed curve).

4.3. Solution to the transversal and longitudinal gluon propagators

In Figs. 6 and 7, a similar analysis is presented but now for the gluon propagator. In Fig. 6, the dependence of the propagators

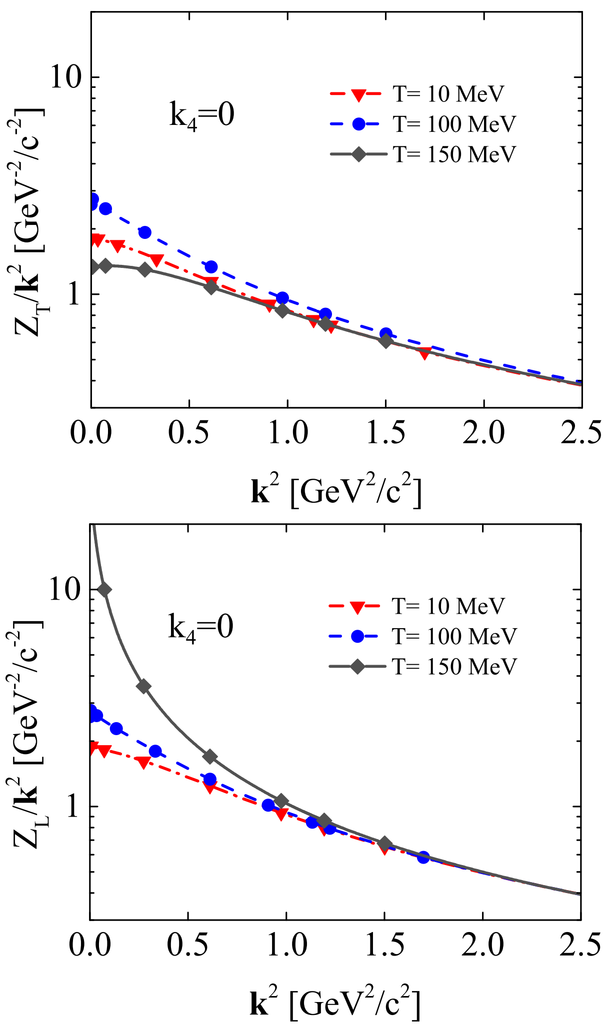

FIG. 6. (color online) The dependence on the three-momentum squared $\mathbf{k}^2$ of the solution to the Dyson–Schwinger equation for the zero Matsubara mode of the transversal $Z_T(k_4, \mathbf{k}^2)/k^2$ and longitudinal $Z_L(k_4, \mathbf{k}^2)/k^2$ gluon propagators, left and right panels, respectively. Solid, dashed and dot-dashed curves correspond to $T = 150$ MeV, $T = 100$ MeV and $T = 10$ MeV, respectively.

for the zero Matsubara mode is displayed as a function of the spatial momentum squared $\mathbf{k}^2$ at several values of the temperature, $T = 10$ MeV, $T = 100$ MeV and $T = 150$ MeV. As in the previous case, the dependence of the transversal, left panel, and longitudinal, right panel, propagators at moderate and large values of $\mathbf{k}^2$ is rather weak. The T-dependence of the propagators is more pronounced in the region of low momenta $\mathbf{k}^2$ where the transversal and longitudinal propagators manifest quite different behaviour as functions of T. While the transversal propagator is not so sensitive to T, the longitudinal one sharply increases with T. This is more evidently seen in Fig. 7, left panel, where the temperature dependence of the Matsubara zero mode is presented at $\mathbf{k}^2 \sim 0$. The steep behaviour at $T \sim T_0$ of the longitudinal propagator is manifested more distinctly. Moreover, we observed that for larger temperatures $T > T_0$, viz. $T \gtrsim 160$ MeV, the iteration procedure no longer converges and the solution to the tDSE for the gluon propagators disappears. This is a direct indication that our approach with the temperature independent effective parameters cannot be extended to large temperatures.

The right panel in Fig. 7 reflects the T-dependence of the gluon propagator at $\mathbf{k}^2 = 0$ and two values of the Matsubara frequency, $n = 0$ and $n = 1$. The different behaviour of the longitudinal propagator at moderate and high temperatures is due to the vanishing fourth component $k_4^2 = 0$ for $n = 0$ and relatively large values of k_4, $k_4^2 = 4\pi^2T^2$, for $n = 1$. Recall that in the tDS equations with the interaction kernels (6)-(9) and the effective formfactors (10)-(12), the fourth components k_4 enter as $\exp(-k_4^2/\omega^2)$, which essentially affect the values of the corresponding propagators at finite n and large T. Since the transverse propagator is less sensitive to the temperature, see left panel in Fig. 7, the dependence on the Matsubara modes is not so strong. This is in fairly good qualitative agreement with the results obtained for the temperature interval ($0 \leq T \leq 150$ MeV) within the FRG framework (see Refs. [10, 11, 15, 36] and references therein quoted) and within the lattice QCD simulations [3, 4, 35], where a noticeable sensitivity of the longitudinal component of the gluon propagator with respect to the deconfining phase transition has been observed.

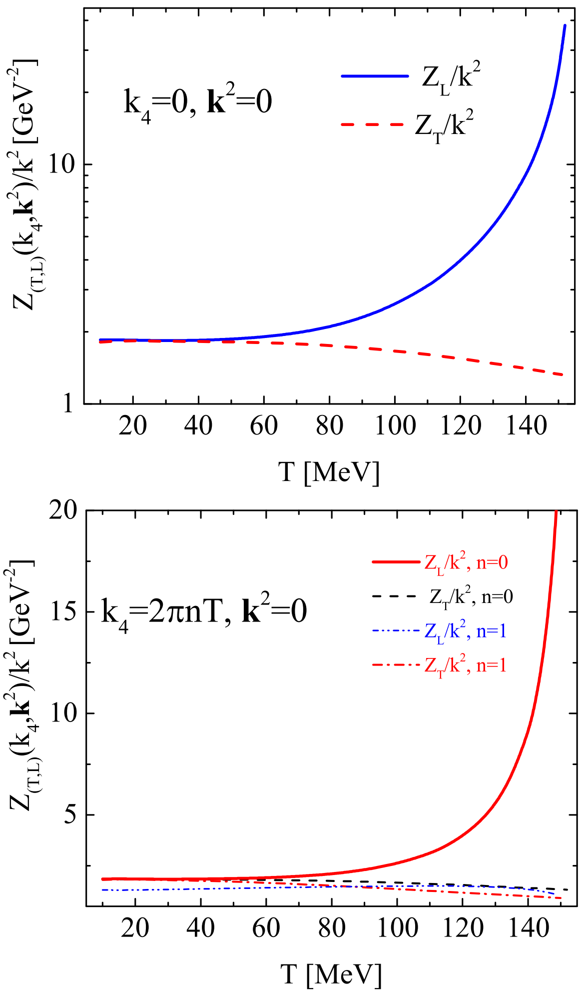

FIG. 7. (color online) The solution of the Dyson–Schwingerequation for the gluon propagators $Z_{L,T}(k_4,\mathbf{k}^2)/k^2$. Left panel: temperature dependence of the zero Matsubara modes of the propagators at $\mathbf{k}^2 = 0$. Solid curve corresponds to the longitudinal propagator, the dashed curve is for the transversal one. Right panel: illustration of the temperature dependence of the transversal and longitudinal propagators for the zero and non-zero Matsubara modes. Solid and dashed lines are those displayed in the left panel, i.e. for $n = 0$. The dot-dot-dashed and dot-dashed lines correspond to longitudinal and transversal propagators at $n = 1$, respectively. Note the *log* scale on the left panel and the linear scale on the right panel.

5. Summary

In summary, we have solved numerically the system of truncated gluon-ghost Dyson–Schwinger equations within the rainbow approximation at zero and finite temperatures. The effective parameters of the interaction kernels were considered temperature independent and taken from the fit of the quark, gluon, and ghost propagators to the SU(2) lattice QCD results in vacuum. We argue that for the zero-Matsubara frequency, $n = 0$, the dependence of the dressing functions on the three-momentum squared $\mathbf{k}^2$ is not sensitive to temperature T in almost the whole range of $\mathbf{k}^2$. Contrarily, a strong dependence on n and T was found at the origin $\mathbf{k}^2 = 0$. We found that, with the effective parameters fixed from vacuum calculations, the iteration procedure of solving the tDSE does not converge at large enough temperatures, $T > T_0$, where $T_0 \sim 150 - 160$ MeV. In the vicinity of T_0, the longitudinal gluon propagator sharply increases, whereas the transversal one does not exhibit irregularities. This means that if one searches for some gluon phase transitions, the most appropriate quantity to study is the temperature dependence of the longitudinal propagators. The presented investigations can be considered as the first step in further, more reliable, analysis of the T-dependence of gluon and ghosts propagators. The obtained solution to the tDSE can be directly included into the Bethe–Salpeter equations to perform studies of the behaviour of glueballs as two-gluon bound states in hot and dense matter.

Acknowledgments

A bulk of numerical calculations were performed on the basis of the HybriLIT heterogeneous computing platform [37] (supercomputer “Govorun”, LIT, JINR).

References

[1] V. G. Bornyakov, E.-M. Ilgenfritz, C. Litwinski, M. Müller-Preussker and V. K. Mitrjushkin, Landau gauge ghost propagator and running coupling in SU(2) lattice gauge theory, Phys. Rev. D **92**, 074505 (2015).

[2] V. G. Bornyakov, V. K. Mitrjushkin and M. Müller-Preussker, SU(2) lattice gluon propagator: continuum limit, finite-volume effects and infrared mass scale m_{IR}, Phys. Rev. D **81**, 054503 (2010).

[3] R. Aouane, V. G. Bornyakov, E. M. Ilgenfritz, V. K. Mitrjushkin, M. Muller-Preussker and A. Sternbeck, Landau gauge gluon and ghost propagators at finite temperature from quenched lattice QCD, Phys. Rev. D **85**, 034501 (2012).

[4] E. M. Ilgenfritz, J. M. Pawlowski, A. Rothkopf and A. Trunin, Finite temperature gluon spectral functions from $N_f = 2+1+1$ lattice QCD, Eur. Phys. J. C **78**, no.2, 127 (2018).

[5] P. O. Bowman, U. M. Heller, D. B. Leinweber, M. B. Parappilly, A. Sternbeck, L. von Smekal, A. G. Williams and J. Zhang, Scaling behavior and positivity violation of the gluon propagator in full QCD, Phys. Rev. D **76**, 094505 (2007).

[6] P. O. Bowman, U. M. Heller, D. B. Leinweber, M.B. Parappilly amd A. G. Williams, Unquenched Gluon Propagator in Landau Gauge, Phys. Rev. D **70**, 034509 (2004).

[7] M. Albanese et al. [Ape Collaboration], Glueball Masses and the Loop Loop Correlation Functions, Phys. Lett. B **197**, 400 (1987).

[8] Y. Chen, A. Alexandru, S. Dong, T. Draper, I. Horvath et al. Glueball spectrum and matrix elements on anisotropic lattices, Phys. Rev. D **73**, 014516 (2006).

[9] C. J. Morningstar and M. J. Peardon, The Glueball spectrum from an anisotropic lattice study, Phys. Rev. D **60**, 034509 (1999).

[10] N. Dupuis, L. Canet, A. Eichhorn, W. Metzner, J. M. Pawlowski, M. Tissier and N. Wschebor, The nonperturbative functional renormalization group and its applications, Phys. Rept. **910**, 1 (2021).

[11] A. K. Cyrol, M. Mitter, J. M. Pawlowski, N. Strodthoff, Non-perturbative finite temperature Yang-Mills theory, Phys. Rev. D**97**, 054015 (2018).

[12] M. A. Shifman, A. I. Vainshtein, and V. I. Zakharov, QCD and Resonance Physics. Theoretical Foundations, Nucl. Phys. B **147**, 385 (1979).

[13] E. V. Shuryak, The Role of Instantons in Quantum Chromodynamics. 2. Hadronic Structure, Nucl. Phys. B **203**, 116 (1982).

[14] C. Fischer, QCD at finite temperature and chemical potential from Dyson-Schwiger equations, Progr. Part. Nucl. Phys., **105**, 1 (2019).

[15] A. Maas, Gauge bosons at zero and finite temperature, Phys. Repts., **524**, 203 (2013).

[16] A. Das, Finite Temperature Field Theory, World Scientific Publishing, 1997.

[17] R. Alkofer, P. Watson, H. Weigel, Mesons in a Poincare covariant Bethe–Salpeter approach, Phys. Rev. D **65**, 094026 (2002).

[18] C. Roberts, V. Bnagwat, A. Holl, S. Wringht, Aspects of Hadron Physics, Eur. Phys. J. ST **140**, 53 (2007).

[19] P. Maris, P. C. Tandy, Bethe–Salpeter study of vector meson masses and decay constants, Phys. Rev. C **60**, 055214 (1999).

[20] S. M. Dorkin, L. P. Kaptari and B. Kämpfer, Accounting for the analytical properties of the quark propagator from the Dyson–Schwinger equation, Phys. Rev. C **91**, 055201 (2015).

[21] M. Blank, A. Krassnigg, The QCD transition temeprature in a Dyson–Schwinger-equation context, Phys. Rev. D **82**, 034006 (2010).

[22] S. Dorkin, M. Viebach, L. Kaptari, B. Kämpfer, Extending the truncated Dyson–Schwinger equatin to finite temperatures, J. Mod. Phys. **7**, 2071 (2016).

[23] S. Dorkin, L. P. Kaptari, B. Kämpfer, Pseudo-scalar $q\bar{q}$ bound states at finite temperatures, Few Body Syst. **60**, 20 (2019).

[24] Si-xue, Lei Chang, Yu-xin Liu, C. Roberts, Quark spectral density and strongly-coupled quark-gluon plasma, Phys. Rev. D **84**, 014017 (2011).

[25] L. von Smekal, A. Hauck and R. Alkofer, The Infrared Behavior of Gluon and Ghost Propagators in Landau Gauge QCD, Phys. Rev. Lett. **79**, 3591 (1997).

[26] L. von Smekal, A. Hauck, R. Alkofer, A solution to coupled Dyson–Schwinger equations for gluons and ghosts in Landau gauge, Ann. Phys. **267**, 1 (1998).

[27] R. Alkofer and L. von Smekal, The Infrared behavior of QCD Green's functions: Confinement dynamical symmetry breaking, and hadrons as

relativistic bound states, Phys. Rept. **353**, 281 (2001).

[28] L. P. Kaptari and B. Kämpfer, "Ghost and Gluon Propagators at Finite Temperatures within a Rainbow Truncation of Dyson–Schwinger Equations," JETP Lett. **114**, 501 (2021).

[29] B. Gruter, R. Alkofer, A. Maas, J. Wambach, Temperature Dependence of Gluon and Ghost Propagators in Landau-Gauge YangвЂ"Mills Theory below the Phase Transition, Eur.Phys.J. C **42**, 109 (2005).

[30] C. W. Bernard, Feynman rules for gauge theories at finite temperature, Phys. Rev. D **9**, 3312 (1974).

[31] D. J. Gross, R. D. Pisarski, J. W. Gibbs, G. Yaffe, QCD and instantons at finite temperature, Rev. Mod. Phys. **53**, 43 (1981).

[32] Varouzhan Baluni, Non-Abehan gauge theories of Fermi systems: Quantum-chromodynamic theory of highly condensed matter, Phys. Rev. D **17**, 202 (1978).

[33] A. Maas, J. Wambach and R. Alkofer, The High-temperature phase of Landau-gauge Yang-Mills theory, Eur. Phys. J. C **42**, 93 (2005).

[34] A. Cucchieri, A. Maas, T. Mendes, Infrared properties of propagators in Landau gauge pure Yang-Mills theory at finite temperature Phys. Rev. D **75**, 07600 (2007).

[35] C. S. Fischer, A. Maas, and J. A. Müller, Chiral and deconfinement transition from correlation functions: SU(2) vs. SU(3), Eur. Phys. J. C **68**, 165 (2010).

[36] Wei-jie Fu, J.M. Pawlowski, F. Rennecke, QCD phase structure at finite temperature and density, Phys. Rev. D **101**, 054032 (2020).

[37] Gh. Adam, M. Bashashin, D. Belyakov, M. Kirakosyan *et al.*, IT-ecosystem of the HybriLIT heterogeneous platform for high-performance computing and training of IT-specialists. The 8th International Conference "Distributed Computing and Grid-technologies in Science and Education" (GRID 2018), Dubna, Russia, September 10-14, 2018, CEUR-WS.org/Vol-2267.